



Tissue- and cell-specific expression of a splice variant in the II-III cytoplasmic loop of *Cacna1b*

Alexandra Bunda , Brianna LaCarubba, Marie Akiki and Arturo Andrade 

Department of Biological Sciences, University of New Hampshire, Durham, NH, USA

Keywords

alternative splicing; BaseScope™; calcium channels

Correspondence

A. Andrade, Department of Biological Sciences, University of New Hampshire, 46 College Road, 214 Rudman Hall. Durham, NH 03824, USA.

Tel: +1 603 862 0015

E-mail: Arturo.Andrade@unh.edu

Alexandra Bunda and Brianna LaCarubba contributed equally to this work

(Received 9 April 2019, revised 19 June 2019, accepted 15 July 2019)

doi:10.1002/2211-5463.12701

Presynaptic Ca_v2.2 (N-type) channels are fundamental for transmitter release across the nervous system. The gene encoding Ca_v2.2 channels, *Cacna1b*, contains alternatively spliced exons that result in functionally distinct splice variants (e18a, e24a, e31a, and 37a/37b). Alternative splicing of the cassette exon 18a generates two mRNA transcripts (+e18a-*Cacna1b* and Δe18a-*Cacna1b*). In this study, using novel mouse genetic models and *in situ* hybridization (BaseScope™), we confirmed that +e18a-*Cacna1b* splice variants are expressed in monoaminergic regions of the midbrain. We expanded these studies and identified +e18a-*Cacna1b* mRNA in deep cerebellar cells and spinal cord motor neurons. Furthermore, we determined that +e18a-*Cacna1b* is enriched in cholecystokinin-expressing interneurons. Our results provide key information to understand cell-specific functions of Ca_v2.2 channels.

Presynaptic Ca_v2.2 (N-type) channels are key mediators of transmitter release across the nervous system. The calcium that enters through Ca_v2.2 channels in response to action potentials triggers transmitter release [1,2]. *Cacna1b* is a multi-exon gene that encodes the Ca_vα₁ pore-forming subunit of Ca_v2.2 channels. The *Cacna1b* pre-mRNA contains more than 40 exons that are spliced during mRNA maturation [3]. Most *Cacna1b* exons are constitutively included in the final *Cacna1b* mRNA; however, some are selectively included through alternative splicing (e18a, e24a, e31a, and 37a/37b) [4]. Alternative splicing of the *Cacna1b* pre-mRNA originates splice variants that are translated into Ca_v2.2 channels with distinct biophysical properties and pharmacological profiles [5,6]. Ca_v2.2 splice variants with differences in activation, inactivation, and current density [7–9], as

well as in their response to neurotransmitters and drugs such as GABA and morphine, have been previously characterized [10,11]. Thus, alternative splicing of the *Cacna1b* pre-mRNA is thought to provide functional diversification to cells that utilize Ca_v2.2 channels to release neurotransmitter.

Among the alternative spliced exons in the *Cacna1b*, pre-mRNA is the cassette exon 18a (e18a) [12]. Alternative splicing of e18a generates two splice variants, +e18a-*Cacna1b* (e18a is included) and Δe18a-*Cacna1b* (e18a is skipped) (Fig. 1A). E18a encodes 21 amino acids within the ‘synprint’ region of the II-III cytoplasmic loop of Ca_v2.2 (LII-III), an essential region for interaction of Ca_v2.2 channels with presynaptic proteins [13–15]. Functionally, +e18a-Ca_v2.2 channels are more resistant to cumulative inactivation induced by

Abbreviations

CA1, *cornu ammonis* 1; CA3, *cornu ammonis* 3; CB1R, cannabinoid receptor 1; CCK, cholecystokinin; CNR1, cannabinoid receptor 1 gene; DCN, deep cerebellar nuclei; DRN, dorsal raphe nuclei; g.c.l., granular cell layer; GAD2, glutamate decarboxylase 2; GAPDH, glyceraldehyde 3-phosphate dehydrogenase; h., hilus; LC, locus coeruleus; m.l., molecular layer; p.c.l., pyramidal cell layer; PN, pyramidal neurons; s.p., *stratum pyramidale*; s.r., *stratum radiatum*; SN, substantia nigra; SNc, substantia nigra *pars compacta*; VTA, ventral tegmental area.

repetitive stimulation and closed-state inactivation than $\Delta e18a$ -Ca_v2.2 channels [9]. Furthermore, +e18a-Ca_v2.2 channels exhibit larger calcium currents relative to $\Delta e18a$ -Ca_v2.2 channels in both mammalian expression systems and neurons [16]. Despite all of this information, very little is known about the functional role of +e18a-*Cacna1b* and $\Delta e18a$ -*Cacna1b* splice variants in the nervous system.

To understand the functional role of +e18a-*Cacna1b* and $\Delta e18a$ -*Cacna1b* splice variants, it is necessary to determine their tissue and cell-type expression. Previous studies have shed light on this. In the adult nervous system, the abundance of +e18a-*Cacna1b* mRNA differs among tissues. Higher levels of +e18a-*Cacna1b* mRNA are observed in dorsal root ganglia, superior cervical ganglia, and spinal cord relative to whole brain [6,16]. Interestingly, the relative abundance between +e18a-*Cacna1b* and $\Delta e18a$ -*Cacna1b* mRNAs also differs among brain subregions. Less than 10% of *Cacna1b* splice variants contain e18a in whole cerebral cortex and hippocampus, whereas 30–60% of *Cacna1b*

splice variants contain e18a in the thalamus, cerebellum, hypothalamus, and midbrain [12]. Within the midbrain, ~80% of *Cacna1b* splice variants contain e18a in monoaminergic regions including the ventral tegmental area (VTA), substantia nigra (SN), dorsal raphe nuclei (DRN), and locus coeruleus (LC) [17].

The expression of +e18a-*Cacna1b* is also cell-specific. +e18a-*Cacna1b* mRNA is enriched in tyrosine hydroxylase-expressing cells of the SN pars compacta (SNc) and VTA [17]. +e18a-*Cacna1b* has also been identified in magnocellular neurosecretory cells of hypothalamus and capsaicin-responsive neurons of dorsal root ganglia [7,18]. The molecular mechanisms underlying the tissue- and cell-specific expression of +e18a-*Cacna1b* and $\Delta e18a$ -*Cacna1b* mRNAs are beginning to be elucidated. The RNA-binding protein, Rbfox2, is a splicing factor that represses e18a by binding an intronic region upstream of this exon [16,19]. Rbfox2 expression and activity depend on the cell type; thus, this would help to explain the cell-specific expression of +e18a-*Cacna1b* and $\Delta e18a$ -*Cacna1b* [20,21].

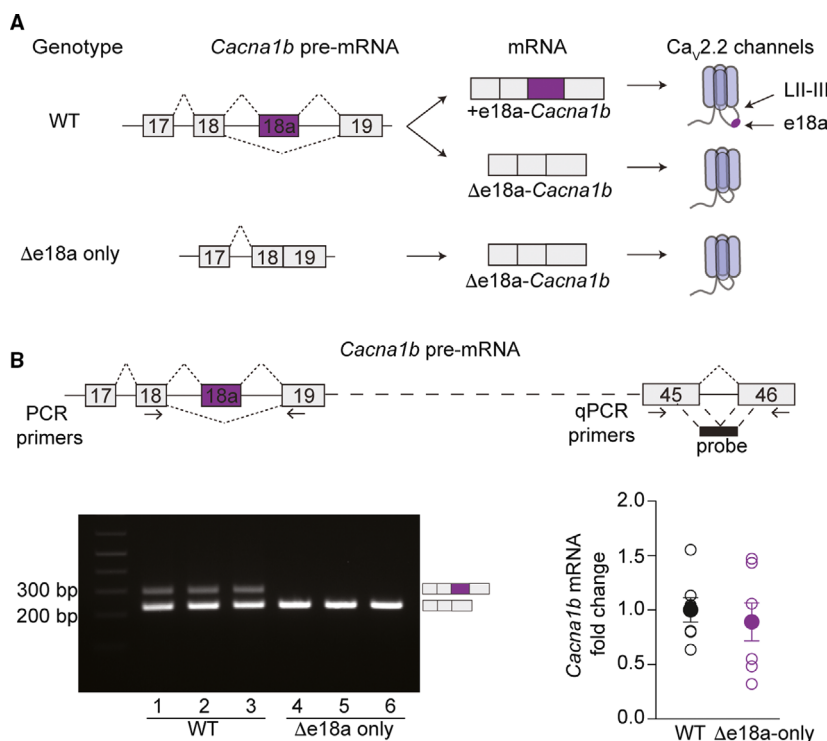


Fig. 1. Targeted deletion of e18a in the *Cacna1b* gene. (A) Schematic of splicing patterns for *Cacna1b* (Ca_v2.2) pre-mRNA in WT and $\Delta e18a$ -only mice. In WT mice, e18a is spliced to generate two mRNA transcripts, +e18a- and $\Delta e18a$ -*Cacna1b*, which in turn are translated into two different Ca_v2.2 channels, +e18a- and $\Delta e18a$ -Ca_v2.2. The *Cacna1b* gene was modified to remove e18a and its flanking intronic regions to generate $\Delta e18a$ -only mice, which generate only the $\Delta e18a$ -Ca_v2.2 splice variant. (B) Top, Schematic of *Cacna1b* pre-mRNA. Arrows indicate the approximate location of RT-PCR primers flanking e18a and qPCR primers in constitutive exons 45 and 46. Black box shows the approximate location of qPCR probe spanning exon junction 45–46. Bottom left, RT-PCR from whole-brain samples of WT and $\Delta e18a$ -only mice. Bottom right, comparison of whole-brain *Cacna1b* mRNA levels between WT and $\Delta e18a$ -only mice. Data are shown as mean (filled symbols) \pm SEM and individual values for biological replicates (empty symbols).

In this study, we utilized a novel version of *in situ* hybridization (ISH) (BaseScope™) and genetic mouse models, to precisely determine the expression of +e18a-*Cacna1b* in the central nervous system. We generated a mouse model that lacks expression of +e18a-*Cacna1b*, thereby expresses only the Δe18a-*Cacna1b* splice variant (Δe18a-only). This mouse was used to control for probe specificity in our BaseScope™ experiments. With these new approaches and tools, we confirmed that +e18a-*Cacna1b* mRNA is expressed in monoaminergic regions (SN, VTA, DRN, and LC). Furthermore, we identified new cell populations that express +e18a-*Cacna1b* mRNA such as cells of the deep cerebellar nuclei (DCN) and spinal cord motor neurons. Finally, using fluorescence-activated cell sorting (FACS) of genetically identified cell populations coupled to RT-PCR, we found that +e18a-*Cacna1b* mRNA is more abundant in cholecystokinin-expressing interneurons (CCK⁺INs) relative to Ca²⁺/calmodulin-dependent protein kinase IIα-expressing projection neurons [CaMKIIα⁺ pyramidal neurons (PNs)].

Materials and methods

Housing conditions

A combination of adult males or females was used in all of our experiments, and no association with sex was found in the amount of e18a in *Cacna1b* in whole brain. Mice were housed with food and water *ad libitum* in temperature-controlled rooms with a 12-h light/dark cycle. All experimental procedures followed the guidelines of the Institutional Animal Care Committee of the University of New Hampshire.

Mouse lines

C57BL/6 wild-type mice were used in our experiments. Mice lacking e18a or Δe18a-only (*Cacna1b*^{tm4.1Dili}) were back-crossed in C57BL/6 (Charles River) background for 6–8 generations, and for details on how this mouse line was generated, see Ref. [16]. To label CCK⁺INs with tdTomato (tdT), we performed intersectional genetic labeling as previously reported [22,23]. We utilized *CCK-Cre* (*Cck*^{tm1.1(cre)Zjh}/J, Jax: 012706) in C57BL/6 background, *Dlx5/6-Flpe* (*Tg(mI56i-flpe)39Fsh*/J, Jax: 010815) in FVB/NJ background, and *Ai65-D* (*B6;129S-Gt(ROSA)26Sort^{m65.1(CAG-tdTomato)Hze}/J*, Jax: 021875) in C57BL/6; I129 background mice. Using these three mouse lines, we generated a triple transgenic line, *CCK-Cre; Dlx5/6-Flpe; Ai65-D* (named *CCK;Dlx5/6;tdT*) as follows: First, *CCK-Cre* mice were crossed with *Dlx5/6-Flpe* two times to produce a dual transgenic mouse (homozygous for *CCK-Cre* and heterozygous for *Dlx5/6-Flpe*). Next, this

dual transgenic mouse line was crossed with homozygous *Ai65-D* mice. From the resulting offspring, we selected only heterozygous mice for the three alleles. To induce the expression of tdT in PNs, we crossed *CaMKIIα-Cre* mice (*B6.Cg-Tg(Camk2a-cre)T29-1Stl*/J, Jax: 005359) in a mixed C57BL6 background with *Ai14* mice (*B6.Cg-Gt(ROSA)26Sort^{tm14(CAG-tdTomato)Hze}/J*, Jax: 007914) in C57BL6. The resulting dual transgenic mouse line *CaMKIIα;tdT* was heterozygous for both alleles.

Genotyping

Conventional toe biopsy was performed on P7-P9 pups. Genomic DNA was extracted using Phire Animal Tissue Direct Kit II (Thermo Fisher Scientific, Waltham, MA, USA, F140WH) according to the manufacturer's instructions. Next, PCR was performed with AmpliTaq Gold® 360 Master Mix (Thermo Fisher Scientific) using the following conditions: a hot start of 95 °C for 10 min, followed by 35 cycles (95 °C, 30 s; 60 °C, 30 s; and 72 °C, 1 min), and final step of 72 °C for 7 min. Primers and expected products are shown in Table 1. Primers were added together to genotype each mouse line.

In situ hybridization (BaseScope™)

Mice were deeply anesthetized with Euthasol (Virbac, Centurion, South Africa, 200-071). Next, mice were transcardially perfused with 1× PBS for 10 min and subsequently with 10% neutral buffered formalin (NBF, ~4% formaldehyde) fixative solution (Sigma, St. Louis, MO, USA, HT501128) for 10 min, and then again with 1× PBS for 10 min. Both PBS and NBF were kept on ice during the perfusion. Brain and spinal cord were immediately removed and postfixed in 10% NBF at 4 °C for 24 h. After washing with 1× PBS, tissue was sequentially dehydrated in 15% and 30% sucrose : PBS solutions for at least 18 h in each sucrose concentration, or until tissue sank to the bottom of the tube. Next, tissue was cryopreserved in optimal cutting temperature compound, or OCT (Fisher, 4585), with isopentane prechilled in dry ice. Twelve micrometer cryosections from brain and spinal cord were collected (Shandon, ThermoFisher Scientific, 77200222) and placed in prechilled 15-mm Netwell™ inserts (Corning, NY, USA, 3478). Sections were allowed to free-float in 1× PBS and mounted on positively charged microscope slides (VWR, 48311-703) using a paintbrush. After air-drying for 10–20 min, sections were incubated at 60 °C in a drying oven for 30 min to aid tissue adhesion to the slides. Before ISH, sections were postfixed in 10% NBF at 4 °C for 15 min and then dehydrated with 50%, 70%, and two rounds of 100% ethanol for 5 min in sequential steps. Slides were air-dried for an additional 5 min before incubating with RNA-scope® hydrogen peroxide solution for 10 min (ACD,

Table 1. Primers to perform genotyping of mouse lines and expected products.

Mouse line	Primers	Expected products
<i>e18a-null</i>	F-MT: CCATGTCTGCTGCCAATATCT F-WT: GCAGCAGAGGTTCTGTTTGC R-C: CTCGGTGCTTTCTGTCTGTCC	Hom: 395 bp Het: 395 and 880 bp WT: 880 bp
<i>CCK-Cre</i>	F-WT1: GGGAGGCAGATAGGATCACA F-MT1: TGGTTTGTCCAACTCAT CAA R: GAGGGGTCGTATGTGTGGTT	Hom: 180 bp Het: 180 bp and 468 bp WT: 468 bp
<i>Dlx5/6-Flpe</i>	F-T1: CAGAATTGATCCTGGGGAGCT ACG R-T1: CCAGGACCTTAGGTGGTGTTC TAC F-C: CAAATGTTGCTTGTCTGGTG R-C: GTCAGTCGAGTGCACAGT TT	Transgene: 406 bp PCR positive control: 200 bp PCR conditions do not differentiate between heterozygous and homozygous mice
<i>Ai14 and Ai65-D</i>	F-WT2: AAGGGAGCTGCAGTGGAG TA R-WT2: CCGAAAATCTGTGGGAAG TC R-MT1: GGCATTAAGCAGCGTAT CC F-MT2: CTGTTCCCTGTACGGCATGG	Hom: 196 Het: 196 and 297 WT: 297
<i>CaMKIIα-Cre</i>	F-T1: GTT CTC CGT TTG CAC TCA GG R-T1: CAG GTT CTT GCG AAC CTC AT F-C: AGT GGC CTC TTC CAG AAA TG R-C: TGC GAC TGT GTC TGA TTT CC	Transgene: ~ 500 bp PCR positive control: 521 bp

All primers are reported in 5' to 3' direction.

Newark, CA, USA, 322381). Next, sections were washed with Milli-Q water and transferred to RNAscope® Target Retrieval solution, preheated to 99 °C for 15 min (ACD, 322000). Sections were briefly washed with Milli-Q water, transferred to 100% ethanol for 3 min, and then placed in drying oven at 60 °C for 30 min. Sections were isolated with a hydrophobic barrier pen (ACD, 310018) and air-dried overnight at room temperature. Following incubation with RNAscope® Protease III for 30 min (ACD, 322381) at 40 °C in the ACD HybEZ™ Hybridization System (ACD, 310010), sections were exposed to a probe spanning e18 and e18a (BaseScope™ Mm-Cacna1b-e18e18a) (ACD, 701151) for 2 h at 40 °C in the ACD HybEZ™ Hybridization System. BaseScope™ Detection Reagents AMP 0–AMP 6 and FastRed (ACD, 322910) were applied according to the manufacturer's instructions and washed using RNAscope® Wash Buffer (ACD, 310091). To visualize nuclei, sections were counterstained in Gill's Hematoxylin I for 2 min at RT (American Master Tech, Lodi, CA, USA, HXGHE). Next, sections were washed with tap water three times, briefly transferred to 0.02% ammonia water, and washed again with tap water. Finally, sections were dried at 60 °C for 15 min and mounted using VectaMount™ mounting medium (Vector Laboratories, Burlingame, CA, USA, H-5000). Phase-contrast images were acquired using an Olympus IX-81 microscope.

Fluorescence-activated cell sorting

Adult *CCK;Dlx5/6;tdT* and *CaMKII α ;tdT* mice were deeply anesthetized with isoflurane. After decapitation, brains were quickly removed and placed on a petri dish with Earl's

balanced salt solution (EBSS) (Sigma, E3024) containing 21 U·mL⁻¹ of papain. Rapid dissection (< 45 s) of cerebral cortex and hippocampus was performed. Then, tissue was dissociated using a modified version of Worthington Papain Dissociation System® (Worthington Biochemical Corporation, Lakewood, NJ, USA, LK003150). After incubating with papain for 45 min at 37 °C on a rocking platform, tissue was triturated with three sequential diameter fire-polished glass pipettes. Next, cell suspensions were centrifuged at 300 *g* for 5 min. After discarding supernatants, pellets were resuspended in 3 mL of EBSS containing 0.1% of ovomucoid protease inhibitor and 0.1% BSA (Worthington, LK003182) to quench papain. Cell suspension was centrifuged at 270 *g* for 6 min and resuspended in EBSS (3 mL). To isolate tdT-expressing cells, we performed FACS in a Sony SH800 flow cytometer using a 561 nm laser to excite and a 570- to 630-nm filter for event selection. At least 300 000 events were collected directly into TRIzol™ LS Reagent (Thermo Fisher Scientific, 10296028). Collection was performed keeping 1 : 3 (v/v) sorted cell suspension: TRIzol™ LS ratio. Cell suspension was kept on ice throughout the sorting session.

RT-PCR and RT-qPCR

Total RNA from tissue was extracted with RNeasy Mini Kit columns (Qiagen, Hilden, Germany, 74134) according to the manufacturer's instructions. Total RNA from sorted cells was extracted using TRIzol LS and isopropanol precipitation with the addition of 30 µg of GlycoBlue® Coprecipitant (Thermo Fisher Scientific, AM9516) to facilitate visualization of RNA pellet. 1 µg (tissue) or 300 ng (sorted

cells) of total RNA was primed with oligo-dT and reverse-transcribed with Superscript IV First-Strand Synthesis System (Thermo Fisher Scientific, 18091050) according to the manufacturer's instructions. To quantify the relative amount of e18a, PCR was performed using AmpliTaq Gold[®] 360 Master Mix (Thermo Fisher Scientific, 4398881) with primers flanking e18a (F: 5'GGCCATTGCTGTGGA CAACCTT and R: 5'CGCAGGTTCTGGAGCCTTAGCT) with the following conditions: hot start at 95 °C for 10 min, 28 cycles (95 °C for 30 s, 60 °C for 30 s, and 72 °C for 1 min), and a final step of 72 °C for 7 min. These sets of primers quantify +e18a- and Δe18a-*Cacna1b* splice variants simultaneously. PCR products were run in 3% agarose gel stained with ethidium bromide, and densitometric analysis was performed using IMAGEJ [24]. This quantification method has been validated before [16]. To confirm band identity, the two bands were cloned and sequenced. To quantify total mRNA levels for *Cacna1b*, glutamate decarboxylase-2 (*Gad-2*) and cannabinoid receptor 1 (*Cnr1*), we performed TaqMan[®] real-time PCR assays (Thermo Fisher Scientific) with the following probes: *Cacna1b*, Mm01333678_m1; *Gad-2*, Mm00484623_m1; *Cnr1*, Mm01212171_s1; and glyceraldehyde 3-phosphate dehydrogenase (*Gapdh*), Mm9999915_g1, which was used as constitutive control. First-strand cDNA was diluted 1 : 5, and 4 μL of this dilution was used in a 20 μL qPCR containing Taq polymerase master mix (Applied Biosystems, Foster City, CA, USA, 4369016) and the predesigned probes mentioned above. RT-qPCRs were run on an ABI 7500 Fast Real-Time PCR System (Applied Biosystems) with the following conditions: 1 cycle 95 °C for 10 min, 4 °C cycles (95 °C for 15 s and 60 °C for 1 min). Each sample from at least five different mice per genotype (biological replicates) was run in triplicate (technical replicates). C_t values were determined by 7500 Software v2.3 (Applied Biosystems). Relative quantification of gene expression was performed with $\Delta\Delta-C_t$ method [25].

Statistical analysis

Two-tailed unpaired Student's *t*-test was performed in Excel (Microsoft).

Results and Discussion

Validation of a mouse model to detect +e18a-*Cacna1b* mRNA in the central nervous system

To determine the localization of +e18a-*Cacna1b* mRNAs in the central nervous system (CNS), we performed a modality of ISH (BaseScope[™]). We used a mouse line with targeted deletion of e18a (Δe18a-only) to control for probe specificity. In this mouse model, DNA sequences between e18 and e19 (e18-e18a intron,

e18a, and e18a-e19 intron) were removed using homologous recombination (Fig. 1A, [16]). To confirm deletion of e18a sequence, we performed RT-PCR in whole-brain samples from WT and Δe18a-only mice. We utilized primers flanking e18a to quantify both +18a- and Δe18a-*Cacna1b* transcripts. Amplicons for each splice variant were resolved on gel electrophoresis based on size (Fig. 1B). In WT whole-brain samples, we observed two bands, ~290 and ~230 bp, corresponding to +18a- and Δ18a-*Cacna1b* transcripts, respectively (Fig. 1B, bottom left panel, lanes 1–3). As expected, the upper band was absent in samples from Δe18a-only mice (Fig. 1B, bottom left panel, lanes 4–6). Next, we tested whether the targeted deletion of e18a alters the overall *Cacna1b* mRNA levels. We quantified total *Cacna1b* mRNA using RT-qPCR with a probe that spans the splice junction between two constitutive exons, e45 and e46 (Fig. 1B, top panel). We found no significant differences in the total amount of *Cacna1b* mRNA between WT and Δe18a-only mice (Fold change relative to control ± SEM: WT = 1 ± 0.12, *n* = 7; e18a-null = 0.89 ± 0.18, *n* = 7. *P* = 0.61. Two-tailed, unpaired, Student's *t*-test. Fig. 1B, right lower panel). Our results show that the e18a sequence was successfully eliminated from the *Cacna1b* gene and that this deletion does not alter the total *Cacna1b* mRNA levels in whole brain. Therefore, this model is ideal to control for the specificity of probes directed to e18a, thereby allowing the localization of +e18a-*Cacna1b* splice variants in CNS tissue.

+e18a-*Cacna1b* mRNA is expressed in substantia nigra and ventral tegmental area

In the CNS, expression of *Cacna1b* is restricted to neurons; however, the cell-specific expression of the *Cacna1b* splice variants has not been fully determined [4]. Previous studies using microdissections and RT-PCR showed that +e18a-*Cacna1b* mRNA is abundantly expressed in SN and VTA [17]. Furthermore, +e18a-*Cacna1b* mRNAs colocalize with tyrosine hydroxylase mRNA in both of these brain areas [17], suggesting that +e18a-*Cacna1b* mRNA is enriched in dopaminergic neurons. Here, we confirmed these findings using BaseScope[™] with a probe designed against the e18a sequence. Briefly, 'Z' probes containing a short complementary region bind to the e18a sequence. This binding leads to the assembly of a signal amplification system, thereby allowing the detection of short RNA sequences (Fig. 2A). In our experiments, we used brain sections from Δe18a-only mice to control for probe specificity. Red signal indicates the presence of +e18a-*Cacna1b* splice variants, and blue indicates

counterstaining with hematoxylin (Hem) (Fig. 2A). Each dot detects a single mRNA molecule. We performed BaseScope™ in midbrain sections of WT and $\Delta e18a$ -only mice. We compared our BaseScope™ images (Fig. 2B, top panels) to conventional ISH images for the dopaminergic marker, *Slc6a3* dopamine transporter, from SN and VTA found in the Allen Mouse Brain Atlas (Fig. 2B, bottom panels) [26]. We observed that staining for e18a follows a pattern similar to *Slc6a3* in the midbrain. No signal for e18a was detected on sections from $\Delta e18a$ -only mice (Fig. 2B, bottom panels). These results confirm previous studies showing that e18a is expressed in SN and VTA regions. It is important to note that we observed +e18a-*Cacna1b* expression in other cells near VTA and SNc; the identity of these cells is currently unknown. Some cells expressing +e18a-*Cacna1b* were also observed in SN pars reticulata.

To our knowledge, antibodies specific for +e18a- $Ca_v2.2$ channels are unavailable. This would help to convincingly show that +e18a- $Ca_v2.2$ channels are present in dopaminergic neurons. However, our use of BaseScope™ with adequate negative controls sheds light on the localization of e18a in the midbrain. Previous results have shown that dopamine release from VTA and SNc heavily relies on $Ca_v2.2$ channels [27,28]. Our studies and mouse models combined with previous functional studies of +e18a- and $\Delta e18a$ - $Ca_v2.2$ channels in mammalian systems and neurons will enable to propose further studies to unveil a potential role of e18a splicing on dopamine release.

Expression of +e18a-*Cacna1b* mRNA in dorsal raphe nuclei and locus coeruleus

DRN and LC contain neurons that release serotonin and norepinephrine, respectively. DRN is located ventral to the cerebral aqueduct (AQ) (Fig. 3A, top right panel). Prior studies showed that +e18a-*Cacna1b* mRNA is expressed in DRN and LC [17]. We next performed BaseScope™ in these brain areas. To guide our analysis, we compared images for conventional ISH staining for the serotonergic marker, *Slc6a4* (serotonin transporter), from the Allen Mouse Brain Atlas (Fig. 3A, top left panel [26]) to our BaseScope™ staining. Signal for e18a was observed ventral to AQ and followed a pattern similar to *Slc6a4*, suggesting that +e18a-*Cacna1b* splice variants are expressed in DRN (Fig. 3A, middle and bottom left panels). Sections of $\Delta e18a$ -only mice in a similar area show little to no signal for e18a (Fig. 3A, middle and bottom right panels). Our results show that e18a is present in the DRN; however, further studies are needed to

determine the cell populations within the DRN that express +e18a-*Cacna1b* mRNA. $Ca_v2.2$ channels are involved in the release of serotonin [27], and $Ca_v2.2$ -null mice show enhanced aggression that has been linked to the control of serotonin neurons excitability [29]. Our results open the possibility that splicing e18a is linked to the activity of the serotonin system.

To determine whether +e18a-*Cacna1b* mRNA is expressed in LC, we stained sections containing the fourth ventricle (V4) and the central lobule of the cerebellum II (CENT2) (Fig. 3B, top panel). We found that the signal for +e18a-*Cacna1b* mRNA is located lateral to V4 (Fig. 3B, middle and bottom panels). This signal is similar to the pattern of expression for *Slc6a2* (norepinephrine transporter, *Net*) observed in ISH images from the Allen Mouse Brain Atlas [26] (Fig. 3B, top panel). Our results suggest that e18a is present in LC, as previously reported [17].

Distribution of +e18a-*Cacna1b* mRNA in cerebellum

In cerebellum, $Ca_v2.2$ channels control the release of neurotransmitter from climbing fibers and parallel fibers synapsing onto Purkinje cells [30–32]. $Ca_v2.2$ channels are also critical for the intrinsic firing of DCN neurons by coupling to calcium-dependent potassium channels [33]. In cerebellum, ~20% of *Cacna1b* splice variants contain e18a [16]. However, the distribution of +e18a-*Cacna1b* splice variant in the cerebellum is unknown. Using the well-defined anatomy of cerebellum as landmark, we determined the expression of e18a in this area. In cerebellar cortex, little e18a signal was observed in the Purkinje cell layer, as well as the molecular and granular layers (*m.l.* and *g.l.*) (Fig. 4A, left panel, inset 1). However, in the DCN, we observed several cell bodies stained for e18a (Fig. 4A, left panel, inset 2 and 3). Very little signal was detected in cerebellar sections from $\Delta e18a$ -only mice (Fig. 4B, right panel and insets 4–6). Our results provide a framework to test whether splicing of e18a influences the firing properties of neuronal populations present in DCN.

Expression of +e18a-*Cacna1b* in spinal cord

$Ca_v2.2$ channels have been previously reported in spinal cord at nociceptive afferents, interneurons, and motor neurons [34]. In spinal cord, we have previously shown that e18a-containing splice variants represent ~55% of the *Cacna1b* pool of transcripts [12]. We next determined the pattern of expression of +e18a-*Cacna1b* in spinal cord. We found very little signal for e18a in laminae I–III (Fig. 5A, insets 1 and 2). In

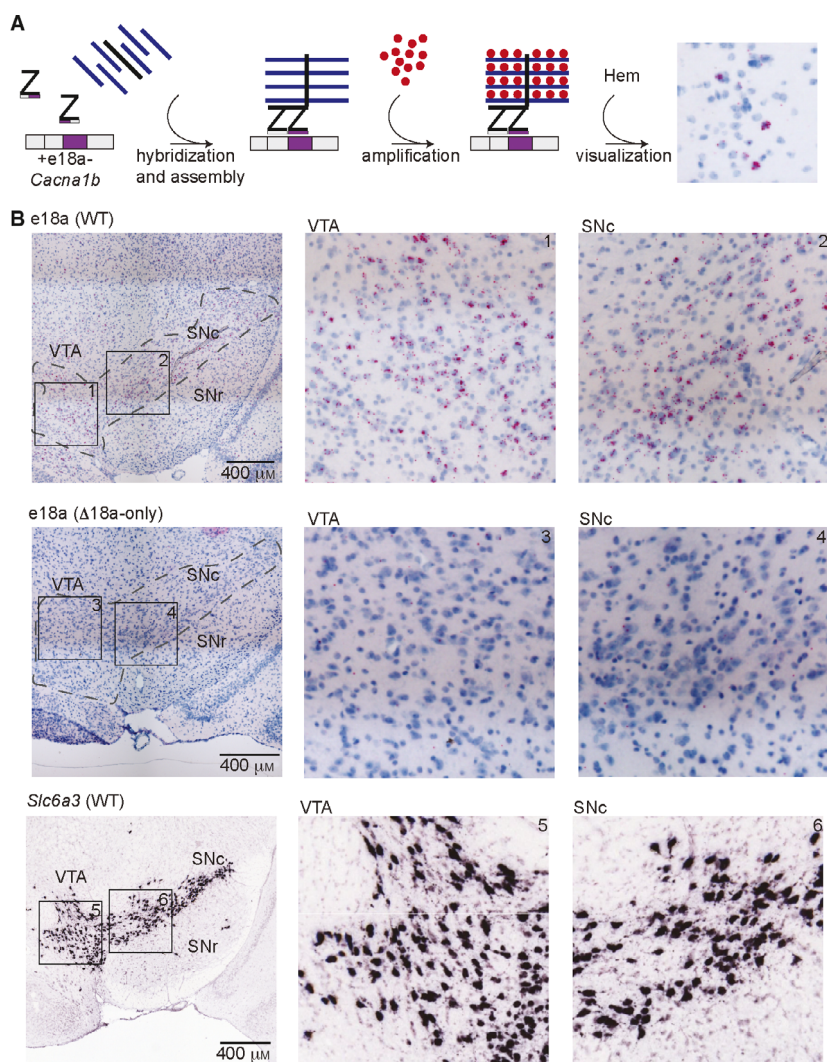


Fig. 2. Localization of e18a-*Cacna1b* in dopaminergic midbrain areas using BaseScope™. (A) Schematic of workflow for BaseScope™. Complementary Z probes were designed to target the junction e18 and e18a. These two independent Z probes bind to the *Cacna1b* mRNA in tandem, thereby allowing the assembly of an amplification complex. Subsequent signal amplification leads to the development of red coloration. Sections were counterstained with Hem. (B) Top panels, BaseScope™ images of VTA and SN from WT mouse brain (left). Insets of VTA and SN (middle and right, respectively). Blue indicates all nuclei stained with Hem. Red dots indicate the presence of +e18a-*Cacna1b* mRNA molecules. Middle panels, BaseScope™ images from areas similar to top panels in Δe18a-only mice. Bottom panels, ISH images for *Slc6a3* in SN and VTA from brain-map.org (left). Black squares represent sections within SN and VTA that were magnified for clarity (insets 1–6). Images credit: Allen Institute. Scale bar = 400 μm.

contrast, large cell bodies in ventral areas (lamina IX) of spinal cord contained > 6 red dots, indicating the presence of e18a (Fig. 5A, inset 2). Note the absence of e18a signal in spinal cord sections of Δe18a-only mice (Fig. 5B, insets 3 and 4). It is well known that dorsal laminae of spinal cord primarily contain neurons that receive sensory inputs from dorsal root ganglia, whereas ventral areas contain circuits that control motor neuron activity. Given that motor neurons in lamina IX have larger cell bodies relative to interneurons [35,36], our results suggest that e18a is expressed

in motor neurons. However, further studies are needed to determine whether +e18a-*Cacna1b* mRNA is more abundant in motor neurons relative to interneurons of spinal cord. Previous studies have shown that some neuromuscular junctions rely on Ca_v2.2 channels to release acetylcholine (phrenic nerve-diaphragm), whereas others utilize almost exclusively Ca_v2.1 (sciatic nerve-tibialis muscle) [37,38]. The cell-specific expression of +e18a-*Cacna1b* mRNA could provide an explanation for this neuromuscular junction-specific role of Ca_v2.2 channels.

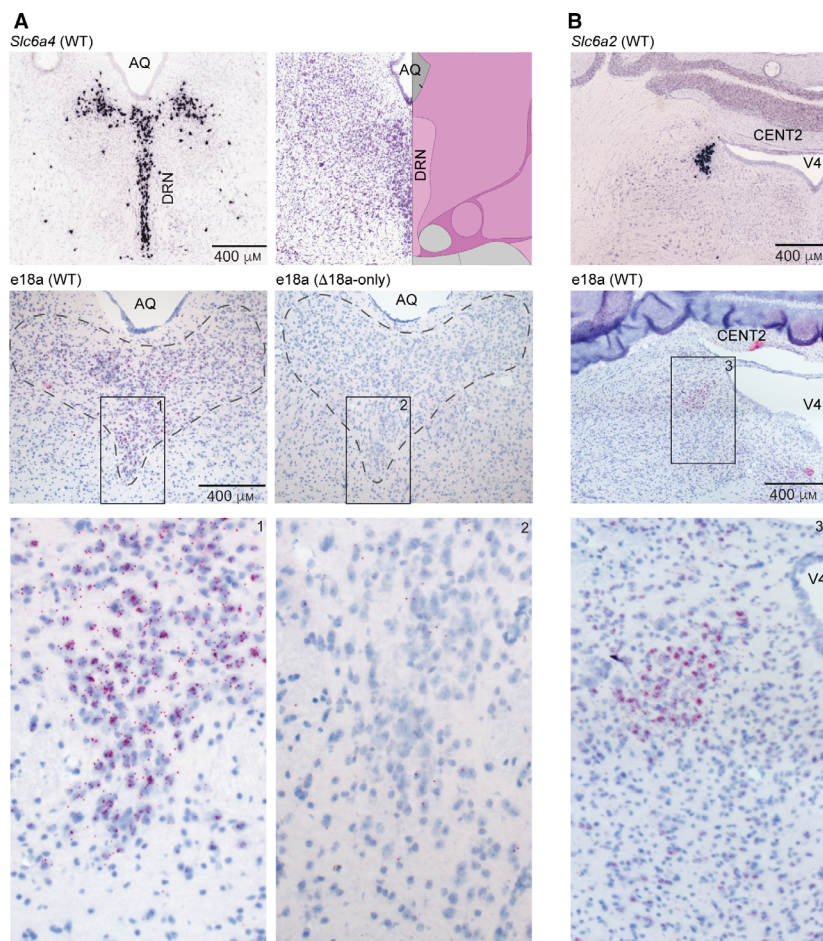


Fig. 3. Localization of e18a-*Cacna1b* in the DRN and LC. (A) Left top panel, ISH images for *Slc6a4* in DRN. AQ. Right top panel, Nissl staining image from brain-map.org showing the approximate location of DRN relative to AQ. Image credit: Allen Institute. Left middle panel, BaseScope™ images from DRN on a section of a WT mouse. Right middle, BaseScope™ images of DRN sections from Δe18a-only mice. (B) Top panel, ISH images for *Slc6a2* in LC. V4 = fourth ventricle. CENT2 = central lobule of the cerebellum 2. Middle panel, BaseScope™ images from WT mice in low and high magnification. Note the presence of e18a lateral to the V4. Red dots indicate the presence of +e18a-*Cacna1b* mRNA. Blue denotes nuclei stained with Hem. Insets are shown and numbered for clarification. Scale bar = 400 μm.

Expression of +e18a-*Cacna1b* splice variants in hippocampus

The functional role of Ca_v2.2 channels in controlling neurotransmission has been extensively described in hippocampal synapses. Interestingly, the distribution of *Cacna1b* splice variants in the hippocampus is unknown. Interneurons reside in *stratum radiatum* (*s.r.*), whereas PN are arranged along *stratum pyramidale* (*s.p.*) of both *cornu ammonis 1* (CA1) and *cornu ammonis 3* (CA3) regions. Using these anatomical landmarks, we determined the expression of e18a in CA1 and CA3 regions. Signal for +e18a-*Cacna1b* mRNA was detected in nuclei of *s.r.* and *s.p.* Interestingly, only a subpopulation of *s.r.* nuclei showed strong signal for e18a in both regions (Fig. 6A,B, left panels). In dentate gyrus (DG), interneurons are located in the hilus (*h.*), whereas granular cells (GC) are localized in the granular cell layer (*g.c.l.*). Here, we observed signal for e18a in several nuclei located in *h.* and *g.c.l.* (Fig. 6C). In sections from Δe18a-only mice, signal for e18a was absent throughout all regions of hippocampus analyzed

(Fig. 6A–C, right panels). We also compared the percentage of cells that show more than one single dot in the DG of hippocampal sections from WT and Δ18a-only mice; less than one dot per cell is likely to be background [39]. We found that ~ 30% of cells in DG from WT contained more than a single dot, compared to ~ 5% the ones from Δ18a-only mice (% cells with more than one dot ± SEM. WT = 29.69 ± 1.23, *n* = 5; Δ18a-only = 4.81 ± 0.17, *n* = 4, *P* < 0.00001, Student's *t*-test). These results further support the specificity of the e18a-*Cacna1b* probe. Based on anatomical landmarks for hippocampus, our results suggest that e18a is broadly distributed among PN, GC, and a subpopulation of interneurons in the hippocampus.

+e18a-*Cacna1b* splice variants are enriched in cholecystinin-expressing interneurons

Ca_v2.2 channels, together with Ca_v2.1 and Ca_v2.3, control transmitter release of excitatory terminals [40]. Ca_v2.2 channels also couple to calcium-dependent potassium channels in PNs, thereby controlling

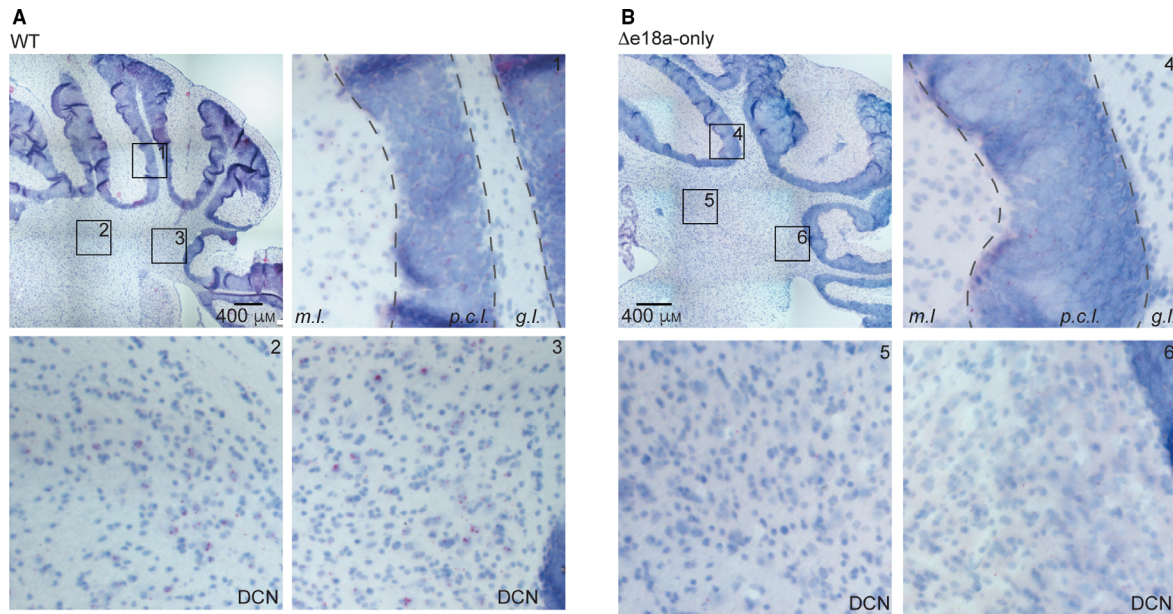


Fig. 4. Localization of +e18a-*Cacna1b* in cerebellum. (A) BaseScope™ images from cerebellum of WT. Insets 1, 2, and 3 indicate magnified areas. Inset 1 represents cerebellar cortex. Layers of the cerebellar cortex are shown: *m.l.*, *p.c.l.*, and *g.l.* Inset 2 and 3 represent deep cerebellar areas. Red dots indicate the presence of +e18a-*Cacna1b* mRNAs. Blue denotes nuclei stained with Hem. (B), BaseScope™ images from cerebellar areas similar to (A) from $\Delta e18a$ -only mice. Inset 4 represent cerebellar cortex and insets 2 and 3 the deep cerebellar areas. Scale bar = 400 μm .

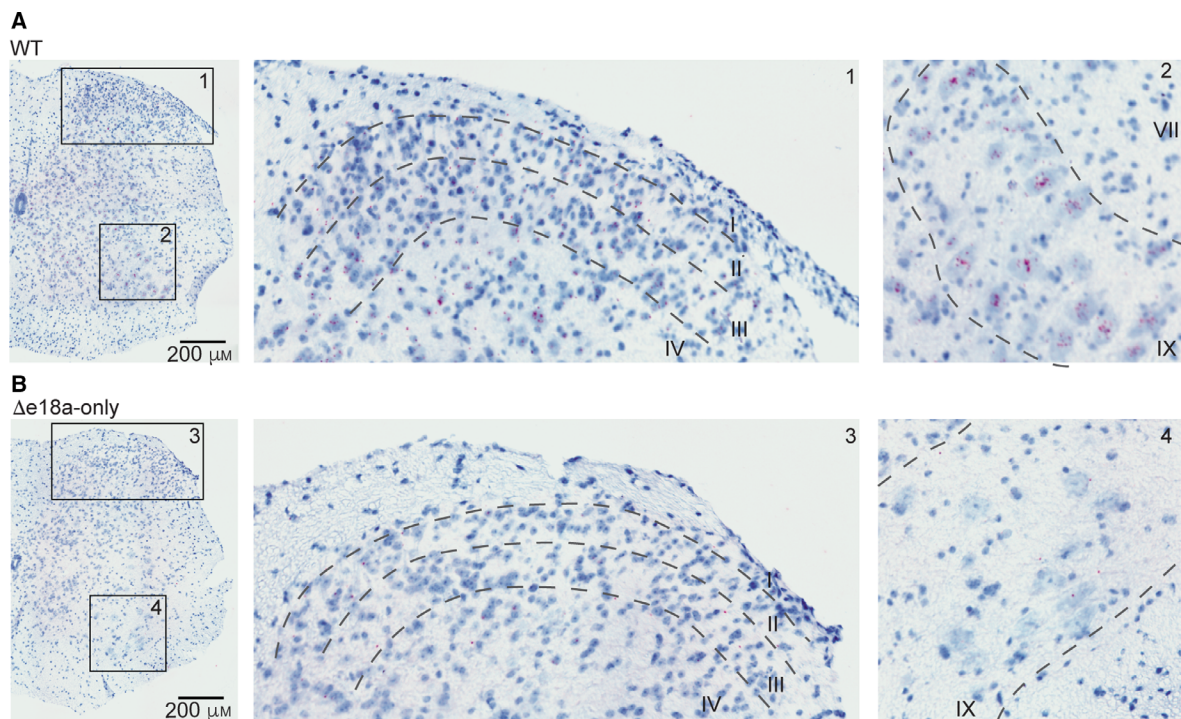


Fig. 5. Distribution of +e18a-*Cacna1b* in spinal cord. (A) BaseScope™ images of spinal cord from WT mice. Inset 1 represents sensory areas containing laminae I-IV. Inset 2 represents motor areas containing laminae VII and IX. Red dots are localized in large nuclei in motor areas. Blue denotes counterstaining with Hem. (B) BaseScope™ images of similar regions as described in A, but in $\Delta e18a$ -only mice. Insets 3 and 4 represent sensory and motor areas of the spinal cord, respectively. Scale bar = 200 μm .

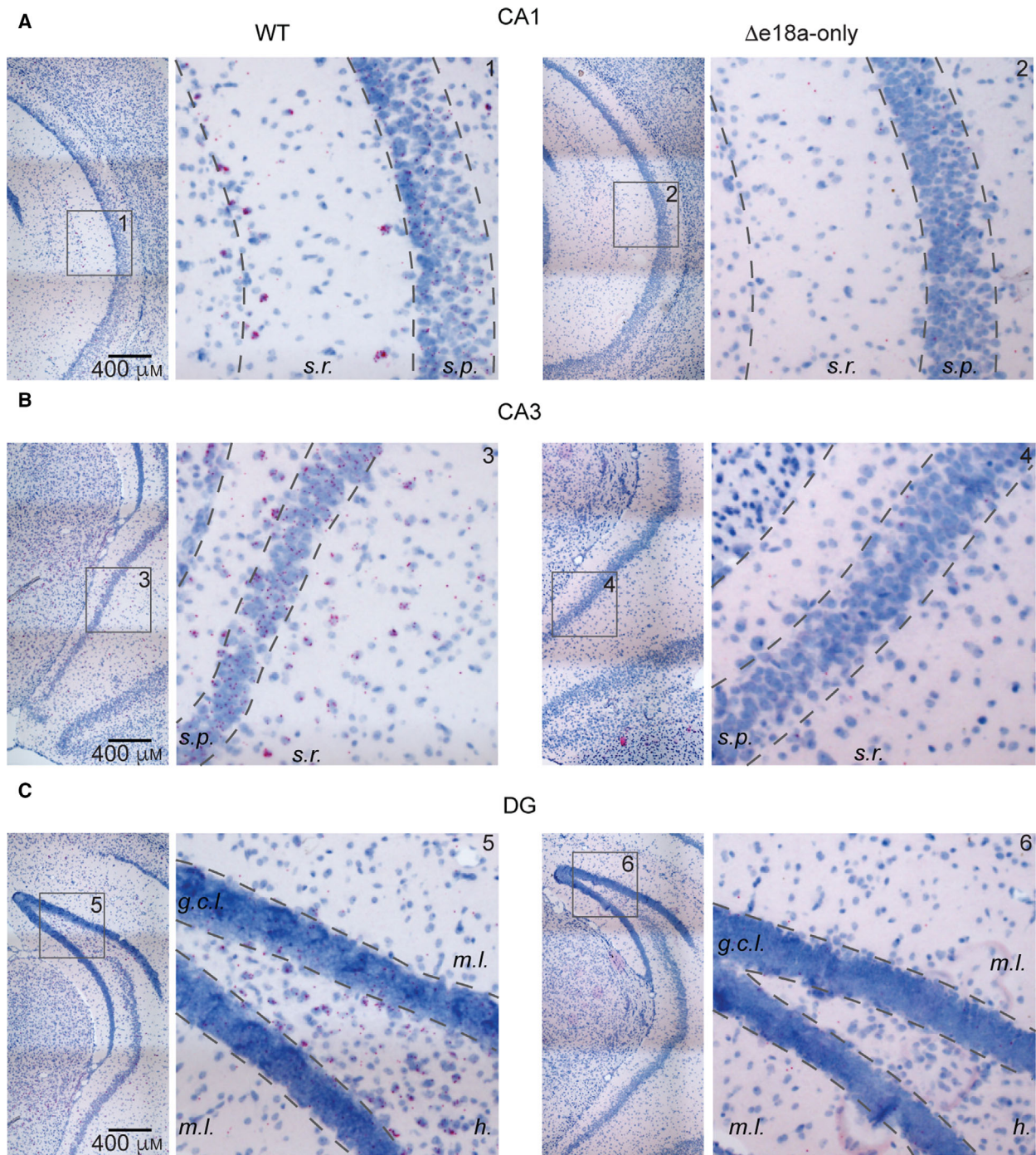


Fig. 6. Localization of *e18a-Cacna1b* in hippocampus. (A) Left, BaseScope™ images of CA1 region of ventral hippocampus in WT mice. Note the presence of red dots in both *s.r.* and *s.p.*. Right, similar to left, but in sections of $\Delta e18a$ -only mice. (B) Left, BaseScope™ images of CA3 region of ventral hippocampus in WT mice. Right, similar to left but in CA3 region of sections from $\Delta e18a$ -only mice. (C) Left, representative images of DG of WT mice stained for *e18a*. DG layers are shown molecular layer (*m.l.*), *h.*, and *g.c.l.* Right, similar to left for $\Delta e18a$ -only mice. In all images, red dots are indicative of the presence of *e18a*, and blue denotes counterstaining of nuclei with Hem. Insets are numbered for clarity. Scale bar = 400 μm.

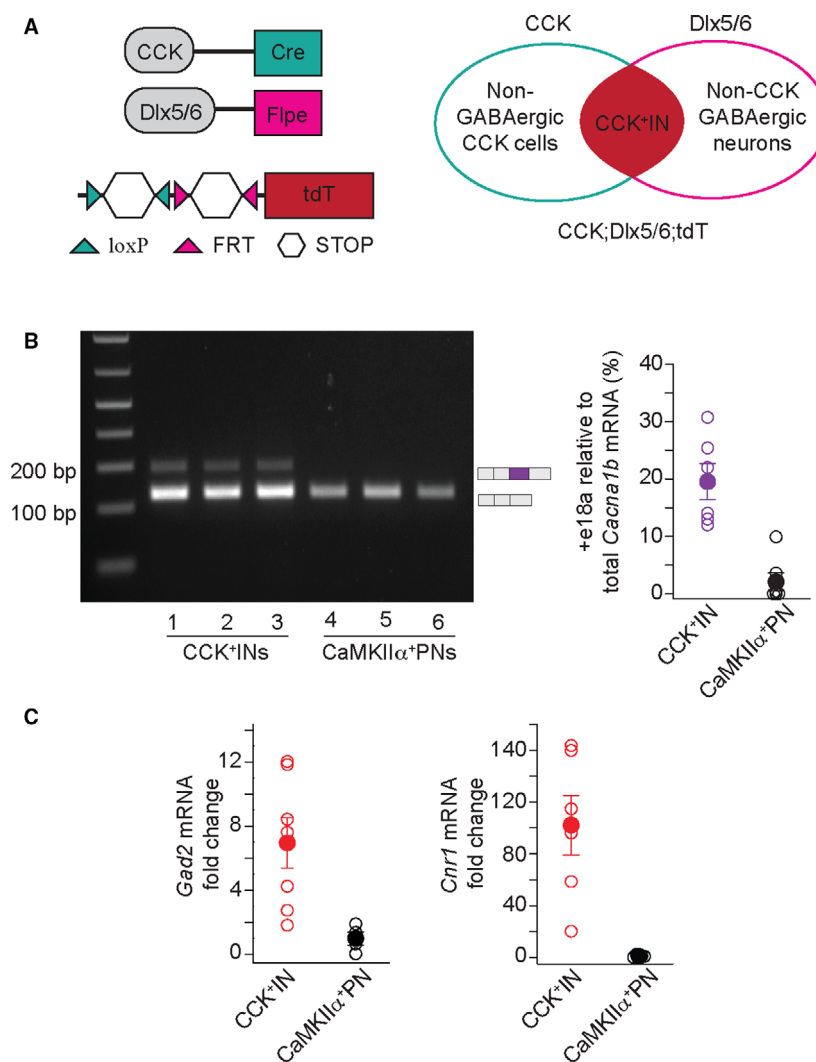


Fig. 7. +e18a-*Cacna1b* mRNA is enriched in CCK⁺INs. (A) Intersectional genetic labeling of CCK⁺INs. Cre recombinase is expressed from the CCK promoter active in CCK interneurons and projection neurons, whereas Flpe recombinase is expressed from the Dlx5/6 promoter active in forebrain GABAergic interneurons. The tdT allele present in Ai65-D mouse contains two STOP codons (white hexagons) flanked by loxP and FRT sites. In a mouse with these three alleles, the combined action of Cre-loxP and Flpe-FRT systems removes both STOP codons allowing expression of tdT in GABAergic CCK⁺INs, but not in PN. (B) Left panel, representative gel of RT-PCR in RNA purified from sorted CCK⁺INs and CaMKII α ⁺PNs. Right panel, comparison of +e18a-*Cacna1b* relative to total *Cacna1b* mRNA in CCK⁺IN and CaMKII α ⁺PN. (C) Validation of sorted cells. Total amounts for glutamate decarboxylase 2 (*Gad2*) and *Cnr1* mRNA were compared between CCK⁺INs and CaMKII α ⁺PNs using RT-qPCR. Data are shown as mean (filled symbols) \pm SEM and the averages of individual biological replicates (empty symbols).

neuronal firing [41]. Furthermore, CCK⁺INs in *s.r.* of CA1 and CA3, and *h.* of DG heavily rely on Ca_v2.2 channels to release GABA [42]. To determine the cell-specific pattern of expression for +e18a-*Cacna1b* mRNA, we compared the relative amounts of +e18a- and Δ e18a-*Cacna1b* mRNAs in CCK⁺INs and PNs by combining genetic labeling, FACS, and RT-PCR. To label CCK⁺IN, we used genetic intersectional labeling with Cre and FLPe recombinases, which resulted in the expression of tdT in CCK⁺INs (Fig. 7A and see Methods). To identify PNs, mice expressing Cre recombinase from the CaMKII α promoter were crossed with mice containing tdT with an upstream floxed STOP codon (CaMKII α ;tdT) [43]. Next, we performed FACS on dissociated tissue from cortex and hippocampus of CCK;Dlx5/6;tdT and CaMKII α ;tdT mice. Total RNA was extracted and reverse-transcribed to quantify the

relative amounts of +e18a- and Δ e18a-*Cacna1b* mRNA. We found that *Cacna1b* splice variants that contain e18a are more abundant in CCK⁺INs relative to CaMKII α ⁺PNs (% e18a relative to total *Cacna1b* mRNA, mean \pm SEM: CCK⁺INs = 19.5 \pm 2.5, n = 7; CaMKII α ⁺PNs = 2.5 \pm 1.7, n = 8. n represents the number of mice. P = 0.006, Student's *t*-test. Fig. 7B). To validate the RNA extracted from sorted cell populations, we quantified *Gad-2* mRNA in both CCK⁺INs and CaMKII α ⁺PNs. As expected, CCK⁺INs express higher levels of *Gad-2* mRNA relative to CaMKII α ⁺PNs (% fold change, mean \pm SEM. CCK⁺INs = 6.9 \pm 1.57, n = 7; CaMKII α ⁺PNs = 1 \pm 0.41, n = 5. P = 0.02, Student's *t*-test. Fig. 7C, left panel). Several groups have reported that CCK⁺INs are enriched with cannabinoid receptor 1 (*Cnr1*) mRNA [44–46]; therefore, to further validate our cell sorting, we compared the levels of *Cnr1* mRNA

between CCK⁺INs and CaMKII α ⁺PNs. We found that CCK⁺INs express significantly higher levels of *Cnr1* than CaMKII α ⁺PNs (% fold change, mean \pm SEM. CCK⁺IN = 102 \pm 23.0, n = 7; CaMKII α ⁺PNs = 1.0 \pm 0.30, n = 8, P = 0.0002, Student's t -test. Fig. 7C, right panel). Taken together, our results strongly suggest that +e18a-*Cacna1b* pre-mRNA is expressed at higher levels in CCK⁺INs relative to CaMKII α ⁺PNs.

With our current results, we are unable to discard the possibility that e18a-*Cacna1b* is also present in other types of GABAergic interneurons in cortex and hippocampus. However, we focus on CCK⁺INs because 100% of GABA release relies on Ca_v2.2 channels; therefore, the functional significance of e18a-*Cacna1b* has high potential [42]. Furthermore, this type of interneurons are linked to mood disorders [47,48], express relatively high levels of the cannabinoid receptor protein (CB1R) [49], and contribute to the behavioral tolerance of tetrahydrocannabinol [50]. Given that CB1R agonists downregulate Ca_v2.2 channels to inhibit GABA release in CCK⁺INs, our findings suggest an anatomical link between e18a splicing in *Cacna1b* and the effects of CB1R agonists of transmitter release. CCK⁺INs in hippocampus show robust asynchronous release and spontaneous release that relies on Ca_v2.2 channels [42]. Due to the slower inactivation rates and positive shift in voltage-dependent inactivation of +18a-Ca_v2.2 channels relative to Δ 18a-Ca_v2.2 channels, it is possible that inclusion of e18a in this neuronal type enhances asynchronous and spontaneous release.

Acknowledgements

This work was supported by the National Institute of Mental Health (grant number, R00MH099405). We thank Sylvia Denome for generating the Δ 18a-only mice, Diane Lipscombe Lab for their advice on Base ScopeTM, and Shayna Mallat for meaningful comments on this manuscript.

Conflict of interest

The authors declare no conflict of interest.

Author contributions

AB performed all ISH experiments. BL performed cell-sorting experiments. MA assisted in cell sorting and ISH. All authors wrote the manuscript. AA designed the study.

References

- Catterall WA (2000) Structure and regulation of voltage-gated Ca²⁺ channels. *Annu Rev Cell Dev Biol* **16**, 521–555.
- Catterall WA (2011) Voltage-gated calcium channels. *Cold Spring Harb Perspect Biol* **3**, a003947.
- Lipscombe D, Allen SE and Toro CP (2013) Control of neuronal voltage-gated calcium ion channels from RNA to protein. *Trends Neurosci* **36**, 598–609.
- Lipscombe D and Andrade A (2015) Calcium channel Ca_v α ₁ splice isoforms - tissue specificity and drug action. *Curr Mol Pharmacol* **8**, 22–31.
- Lipscombe D, Andrade A and Allen SE (2013) Alternative splicing: functional diversity among voltage-gated calcium channels and behavioral consequences. *Biochim Biophys Acta* **1828**, 1522–1529.
- Gray AC, Raingo J and Lipscombe D (2007) Neuronal calcium channels: splicing for optimal performance. *Cell Calcium* **42**, 409–417.
- Bell TJ, Thaler C, Castiglioni AJ, Helton TD and Lipscombe D (2004) Cell-specific alternative splicing increases calcium channel current density in the pain pathway. *Neuron* **41**, 127–138.
- Lin Z, Lin Y, Schorge S, Pan JQ, Beierlein M and Lipscombe D (1999) Alternative splicing of a short cassette exon in alpha1B generates functionally distinct N-type calcium channels in central and peripheral neurons. *J Neurosci* **19**, 5322–5331.
- Thaler C, Gray AC and Lipscombe D (2004) Cumulative inactivation of N-type Ca_v2.2 calcium channels modified by alternative splicing. *Proc Natl Acad Sci USA* **101**, 5675–5679.
- Andrade A, Denome S, Jiang YQ, Marangoudakis S and Lipscombe D (2010) Opioid inhibition of N-type Ca²⁺ channels and spinal analgesia couple to alternative splicing. *Nat Neurosci* **13**, 1249–1256.
- Raingo J, Castiglioni AJ and Lipscombe D (2007) Alternative splicing controls G protein-dependent inhibition of N-type calcium channels in nociceptors. *Nat Neurosci* **10**, 285–292.
- Pan JQ and Lipscombe D (2000) Alternative splicing in the cytoplasmic II-III loop of the N-type Ca channel alpha 1B subunit: functional differences are beta subunit-specific. *J Neurosci* **20**, 4769–4775.
- Bezprozvanny I, Zhong P, Scheller RH and Tsien RW (2000) Molecular determinants of the functional interaction between syntaxin and N-type Ca²⁺ channel gating. *Proc Natl Acad Sci USA* **97**, 13943–13948.
- Sheng ZH, Rettig J, Takahashi M and Catterall WA (1994) Identification of a syntaxin-binding site on N-type calcium channels. *Neuron* **13**, 1303–1313.
- Sheng ZH, Rettig J, Cook T and Catterall WA (1996) Calcium-dependent interaction of N-type calcium

- channels with the synaptic core complex. *Nature* **379**, 451–454.
- 16 Allen SE, Toro CP, Andrade A, López-Soto EJ, Denome S and Lipscombe D (2017) Cell-specific RNA binding protein Rbfox2 regulates CaV2.2 mRNA exon composition and CaV2.2 current size. *eNeuro* **4**, e0332-16.
 - 17 Ghasemzadeh MB, Pierce RC and Kalivas PW (1999) The monoamine neurons of the rat brain preferentially express a splice variant of alpha1B subunit of the N-type calcium channel. *J Neurochem* **73**, 1718–1723.
 - 18 Wang D and Fisher TE (2014) Expression of CaV2. 2 and splice variants of CaV2. 1 in oxytocin- and vasopressin-releasing supraoptic neurones. *J Neuroendocrinol* **26**, 100–110.
 - 19 Gehman LT, Meera P, Stoilov P, Shiue L, O'Brien JE, Meisler MH, Ares M, Otis TS and Black DL (2012) The splicing regulator Rbfox2 is required for both cerebellar development and mature motor function. *Genes Dev* **26**, 445–460.
 - 20 Jangi M, Boutz PL, Paul P and Sharp PA (2014) Rbfox2 controls autoregulation in RNA-binding protein networks. *Genes Dev* **28**, 637–651.
 - 21 Weyn-Vanhentenryck SM, Mele A, Yan Q, Sun S, Farny N, Zhang Z, Xue C, Herre M, Silver PA, Zhang MQ *et al.* (2014) HITS-CLIP and integrative modeling define the Rbfox splicing-regulatory network linked to brain development and autism. *Cell Rep* **6**, 1139–1152.
 - 22 Taniguchi H, He M, Wu P, Kim S, Paik R, Sugino K, Kvitsiani D, Kvitsani D, Fu Y, Lu J *et al.* (2011) A resource of Cre driver lines for genetic targeting of GABAergic neurons in cerebral cortex. *Neuron* **71**, 995–1013.
 - 23 Whissell PD, Cajanding JD, Fogel N and Kim JC (2015) Comparative density of CCK- and PV-GABA cells within the cortex and hippocampus. *Front Neuroanat* **9**, 124.
 - 24 Schneider CA, Rasband WS and Eliceiri KW (2012) NIH Image to ImageJ: 25 years of image analysis. *Nat Methods* **9**, 671–675.
 - 25 Livak KJ and Schmittgen TD (2001) Analysis of relative gene expression data using real-time quantitative PCR and the 2(-Delta Delta C(T)) method. *Methods* **25**, 402–408.
 - 26 Lein ES, Hawrylycz MJ, Ao N, Ayres M, Bensinger A, Bernard A, Boe AF, Boguski MS, Brockway KS and Byrnes EJ (2007) Genome-wide atlas of gene expression in the adult mouse brain. *Nature* **445**, 168.
 - 27 Beuckmann CT, Sinton CM, Miyamoto N, Ino M and Yanagisawa M (2003) N-type calcium channel alpha1B subunit (Cav2.2) knock-out mice display hyperactivity and vigilance state differences. *J Neurosci* **23**, 6793–6797.
 - 28 Brimblecombe KR, Gracie CJ, Platt NJ and Cragg SJ (2015) Gating of dopamine transmission by calcium and axonal N-, Q-, T- and L-type voltage-gated calcium channels differs between striatal domains. *J Physiol* **593**, 929–946.
 - 29 Kim C, Jeon D, Kim Y-H, Lee CJ, Kim H and Shin H-S (2009) Deletion of N-type Ca²⁺ channel Cav2. 2 results in hyperaggressive behaviors in mice. *J Biol Chem* **284**, 2738–2745.
 - 30 Albeni BC, Ryuji KT, Mcintosh JM, Naisbitt SR, Olivera BM and Fillous F (1993) Localization of [125I] omega-conotoxin GVIA binding in human hippocampus and cerebellum. *NeuroReport* **4**, 1331–1334.
 - 31 Doroshenko PA, Woppmann A, Miljanich G and Augustine GJ (1997) Pharmacologically distinct presynaptic calcium channels in cerebellar excitatory and inhibitory synapses. *Neuropharmacology* **36**, 865–872.
 - 32 Etzion Y and Grossman Y (2000) Pressure-induced depression of synaptic transmission in the cerebellar parallel fibre synapse involves suppression of presynaptic N-type Ca²⁺ channels. *Eur J Neurosci* **12**, 4007–4016.
 - 33 Alviña K and Khodakhah K (2008) Selective regulation of spontaneous activity of neurons of the deep cerebellar nuclei by N-type calcium channels in juvenile rats. *J Physiol* **586**, 2523–2538.
 - 34 Westenbroek RE, Hoskins L and Catterall WA (1998) Localization of Ca²⁺ channel subtypes on rat spinal motor neurons, interneurons, and nerve terminals. *J Neurosci* **18**, 6319–6330.
 - 35 Nicolopoulos-Stournaras S and Iles JF (1983) Motor neuron columns in the lumbar spinal cord of the rat. *J Comp Neurol* **217**, 75–85.
 - 36 Tanabe Y and Jessell TM (1996) Diversity and pattern in the developing spinal cord. *Science* **274**, 1115–1123.
 - 37 Rossoni G, Berti F, La Maestra L and Clementi F (1994) Omega-Conotoxin GVIA binds to and blocks rat neuromuscular junction. *Neurosci Lett* **176**, 185–188.
 - 38 Urbano FJ, Rosato-Siri MD and Uchitel OD (2002) Calcium channels involved in neurotransmitter release at adult, neonatal and P/Q-type deficient neuromuscular junctions (Review). *Mol Membr Biol* **19**, 293–300.
 - 39 Wang F, Flanagan J, Su N, Wang LC, Bui S, Nielson A, Wu X, Vo HT, Ma XJ and Luo Y (2012) RNAscope: a novel in situ RNA analysis platform for formalin-fixed, paraffin-embedded tissues. *J Mol Diagn* **14**, 22–29.
 - 40 Wheeler DB, Randall A and Tsien RW (1994) Roles of N-type and Q-type Ca²⁺ channels in supporting hippocampal synaptic transmission. *Science* **264**, 107–111.
 - 41 Marrion NV and Tavalin SJ (1998) Selective activation of Ca²⁺-activated K⁺ channels by co-localized Ca²⁺ channels in hippocampal neurons. *Nature* **395**, 900–905.

- 42 Hefft S and Jonas P (2005) Asynchronous GABA release generates long-lasting inhibition at a hippocampal interneuron-principal neuron synapse. *Nat Neurosci* **8**, 1319–1328.
- 43 Tsien JZ, Chen DF, Gerber D, Tom C, Mercer EH, Anderson DJ, Mayford M, Kandel ER and Tonegawa S (1996) Subregion- and cell type-restricted gene knockout in mouse brain. *Cell* **87**, 1317–1326.
- 44 Fuzik J, Zeisel A, Máté Z, Calvigioni D, Yanagawa Y, Szabó G, Linnarsson S and Harkany T (2016) Integration of electrophysiological recordings with single-cell RNA-seq data identifies neuronal subtypes. *Nat Biotechnol* **34**, 175–183.
- 45 Lenkey N, Kirizs T, Holderith N, Máté Z, Szabó G, Vizi ES, Hájos N and Nusser Z (2015) Tonic endocannabinoid-mediated modulation of GABA release is independent of the CB1 content of axon terminals. *Nat Commun* **6**, 6557.
- 46 Szabó GG, Lenkey N, Holderith N, András T, Nusser Z and Hájos N (2014) Presynaptic calcium channel inhibition underlies CB₁ cannabinoid receptor-mediated suppression of GABA release. *J Neurosci* **34**, 7958–7963.
- 47 Bartos M and Elgueta C (2012) Functional characteristics of parvalbumin- and cholecystokinin-expressing basket cells. *J Physiol* **590**, 669–681.
- 48 Medrihan L, Sagi Y, Inde Z, Krupa O, Daniels C, Peyrache A and Greengard P (2017) Initiation of behavioral response to antidepressants by cholecystokinin neurons of the dentate gyrus. *Neuron* **95**, 564–576.e4.
- 49 Katona I, Sperlág B, Maglóczy Z, Sántha E, Köfalvi A, Cziráj S, Mackie K, Vizi ES and Freund TF (2000) GABAergic interneurons are the targets of cannabinoid actions in the human hippocampus. *Neuroscience* **100**, 797–804.
- 50 Dudok B, Barna L, Ledri M, Szabó SI, Szabadits E, Pintér B, Woodhams SG, Henstridge CM, Balla GY, Nyilas R *et al.* (2015) Cell-specific STORM super-resolution imaging reveals nanoscale organization of cannabinoid signaling. *Nat Neurosci* **18**, 75–86.